Eur. J. Inorg. Chem. **2015** · ISSN 1099–0682

SUPPORTING INFORMATION

DOI: 10.1002/ejic.201500556
Title: Dioxygen Activation by an in situ Reduced Cu^{II} Hydrazone Complex
Author(s): Christian Radunsky, Jutta Kösters, Matthias C. Letzel, Sivathmeehan Yogendra, Christian Schwickert, Sinja Manck, Biprajit Sarkar, Rainer Pöttgen, Jan J. Weigand, Johannes Neugebauer, Jens Müller*

Table S1. Crystallographic data for compounds **3**, **4**, and **5**.

	3	**4**	**5**
empirical formula	$C_{11}H_{11}Cl_2CuN_3S$	$C_{11}H_{12}ClCuN_3O_2S$	$C_{22}H_{22}Cu_2I_2N_6S_2$
formula weight	351.73	349.29	815.46
crystal system	monoclinic	triclinic	monoclinic
space group	*P* $2_1/n$	*P* –1	*P* $2_1/n$
a, *b*, *c* [Å]	13.5644(8), 7.5806(5), 13.6139(8)	8.2733(5), 8.3001(5), 18.795(1)	8.521(1), 17.726(2), 9.577(1)
α, β, γ [°]	90, 106.533(2), 90	88.137(1), 86.594(1), 89.845(1)	90, 114.835(3), 90
V [Å^3]	1342.9(1)	1287.7(1)	1312.7(3)
Z	4	4	2
ρ_{calcd} [g cm^{-3}]	1.74	1.80	2.06
$\mu(Mo_{K\alpha})$ [mm^{-1}]	2.2	2.1	4.2
crystal size [mm]	0.31 × 0.05 × 0.02	0.6 × 0.3 × 0.3	0.12 × 0.07 × 0.05
temperature [K]	153(2)	153(2)	153(2)
θ_{min}, θ_{max} [°]	1.87, 27.93	1.09, 27.87	2.30, 30.12
hkl range	–17:17, –9:9, –17:17	–10:10, –10:10, –24:24	–12:10, 0:24, 0:13
tot., uniq. data	17809, 3201	13252, 6135	3846, 3846
observed data [$I > 2\sigma(I)$]	2657	5256	3536
N_{ref}, N_{par}	3201, 184	6135, 346	3846, 201
R, wR_2, *S* [$I > 2\sigma(I)$]	0.0313, 0.0744, 1.068	0.0399, 0.1034, 1.041	0.0199, 0.0483, 1.039
min. and max. resd. dens. [e Å^{-3}]	0.64, –0.31	1.47, –0.80	0.76, –0.48

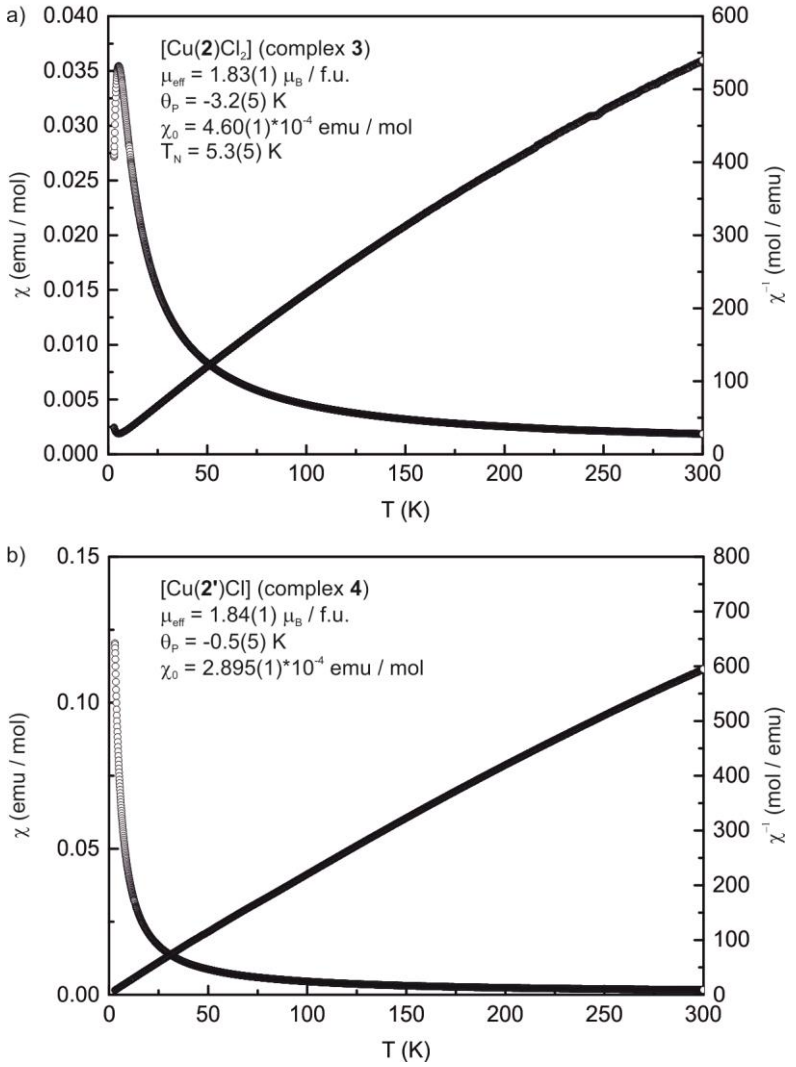

Figure S1. Temperature-dependent magnetic susceptibility of a) complex **3** and b) complex **4** measured in the temperature range from 3 – 300 K with a magnetic flux density of 10 kOe.

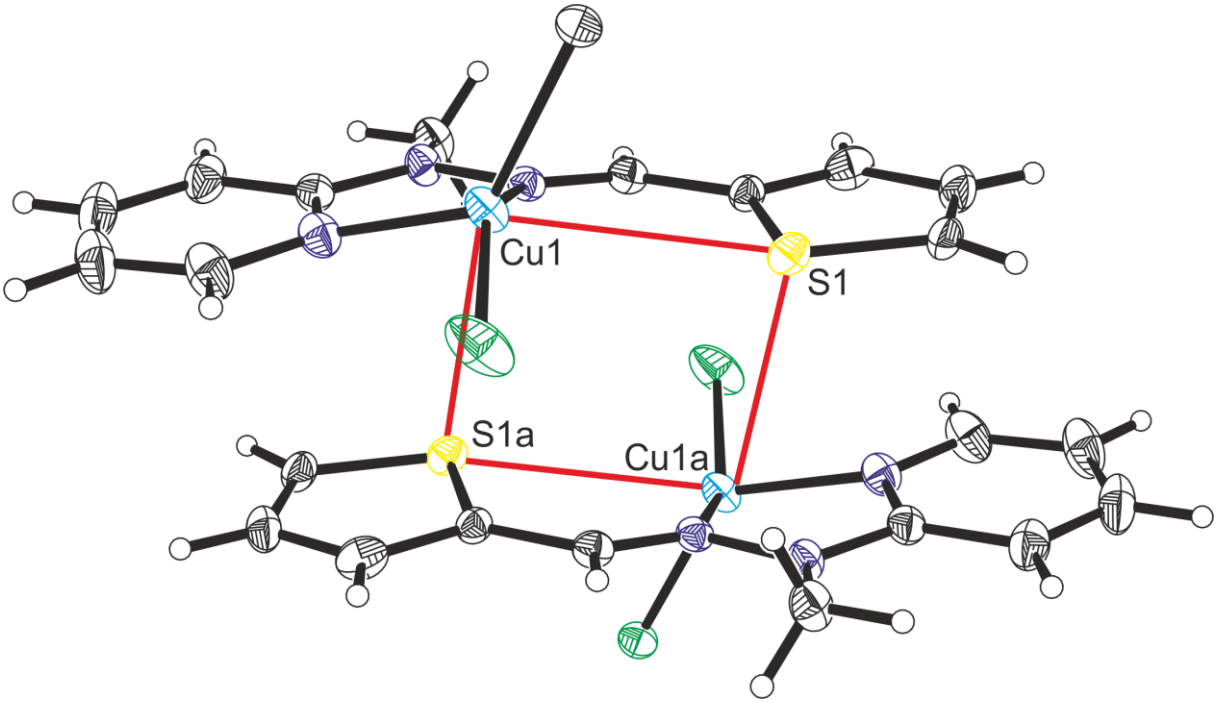

Figure S2. Structural representation of two neighboring molecules of **3**. A possible superexchange pathway explaining the antiferromagnetic behavior below T_N = 5.3(5) K is highlighted in red.

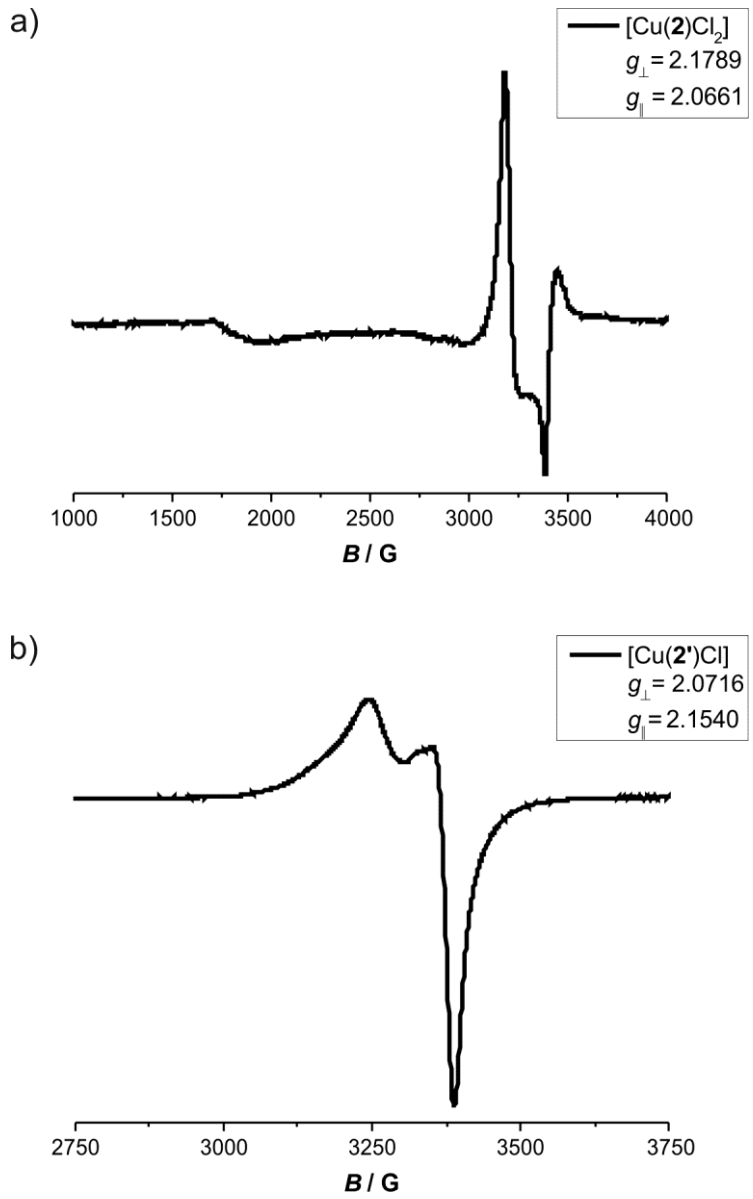

Figure S3. EPR spectra of a) complex **3** and b) complex **4**.

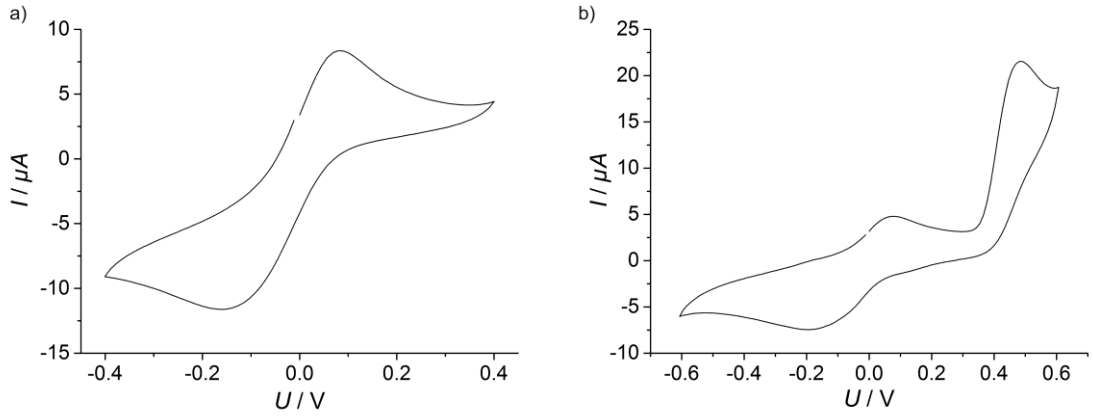

Figure S4. Cyclic voltammograms of a) complex **3** and b) complex **4** in DMSO (conducting salt: 0.15 M tetrabutylammonium hexafluorophosphate, scan rate: 50 mV s^{-1}, data interval: 11.4 mV, reference: ferrocenium/ferrocene). The irreversible oxidation associated with the anodic peak at 484 mV in the case of complex **4** is probably due to a ligand-centered process.

Table S2. Electrochemical data for complexes **3** and **4**.

	Complex **3**	Complex **4**
E^a_{max} / mV	81.4	80.1
E^c_{max} / mV	−162.9	–194.7
$E_{1/2} = (E^a_{max} + E^c_{max})/2$ / mV	–40.8	–57.3
$\Delta E_p = E^a_{max} - E^c_{max}$ / mV	244.3	274.8
i^a_{max} / µA	7.368	2.4443
i^c_{max} / µA	–7.375	–3.3058
$\lvert i^a_{max}/i^c_{max} \rvert$	1.00	0.74

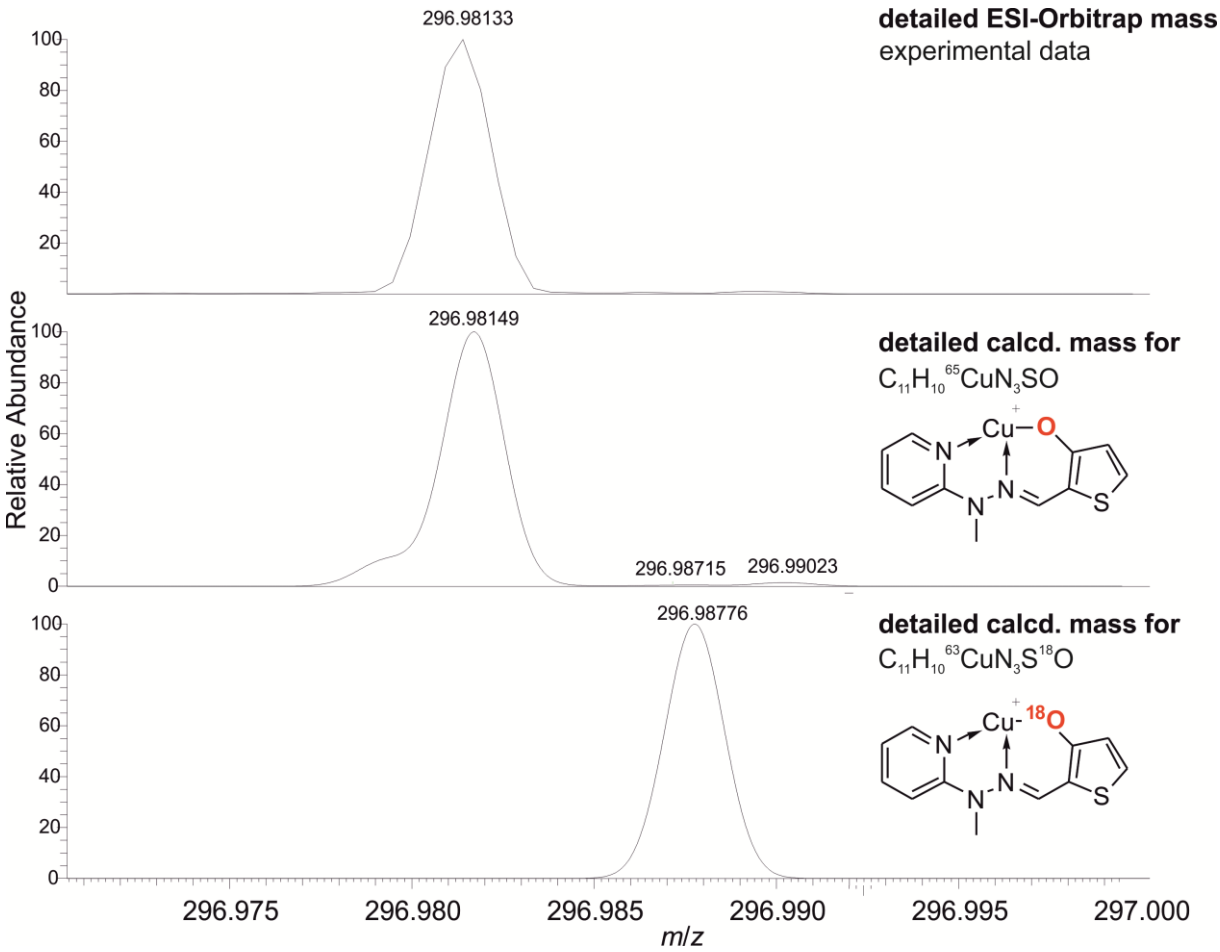

Figure S5. Detailed depiction of the section around *m/z* = 297 of an experimental ESI-Orbitrap mass spectrum of the product obtained by refluxing complex **3** in a mixture of methanol and $H_2{}^{18}O$ (top) and calculated masses of complex **4** (center) and the corresponding ^{18}O species (bottom).

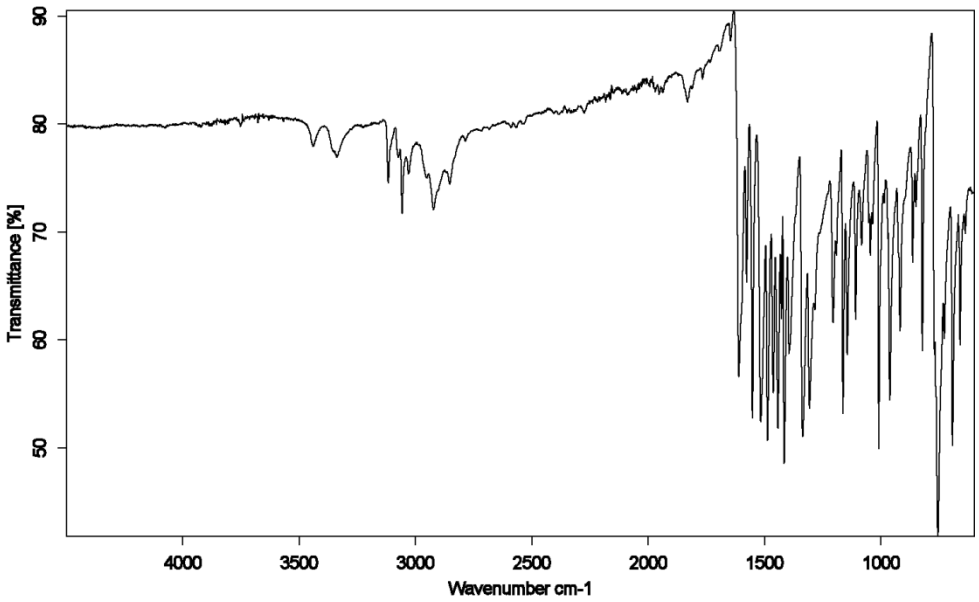

Figure S6. IR spectrum of compound [Cu(**2'**)Cl] **(4)**; sample is slightly moisture sensitive.

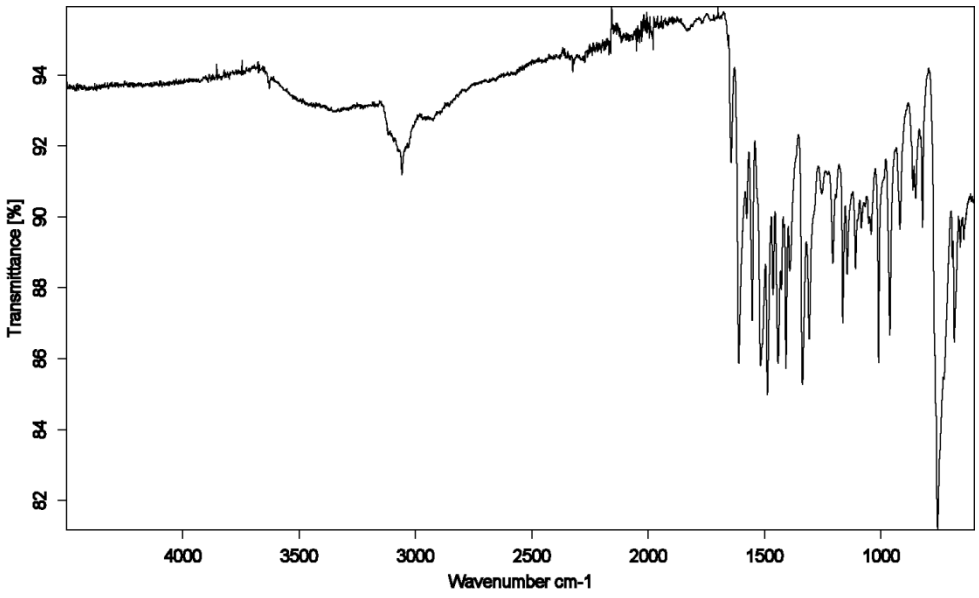

Figure S7. IR spectrum of compound ^{18}O-labeled [Cu(**2'**)Cl] **(4)**.

DFT calculations

The structure optimization for compounds **C3** and **C4** were started from the X-ray crystal structure data of complexes **3** and **4**. In the case of compound **3**, the thienyl moiety is disordered over two positions: Hence, both conformers were treated computationally. In conformer **C3a**, the sulfur atom points towards the copper ion, whereas it points away from the metal center in conformer **C3b**. Both conformers were optimized. For compound **C4**, the crystal structure data file of complex **4** contains two crystallographically independent molecules. Only molecule 1 (assignment according to Table 2 in the manuscript) was treated computationally. The optimized (RI-TPSS/def2-TZVP) structures are shown in Figure S8. As can be seen, the main structural parameters are in good agreement with the experimental data. The calculated energy difference between conformers **C3a** and **C3b** is 1.6 kJ mol^{-1} [1], with **C3b** being slightly more stable. As will be shown below, the UV/Vis spectra of **C3a** and **C3b** are very similar. Hence, we restrict the following discussions to **C3a** and **C4**.

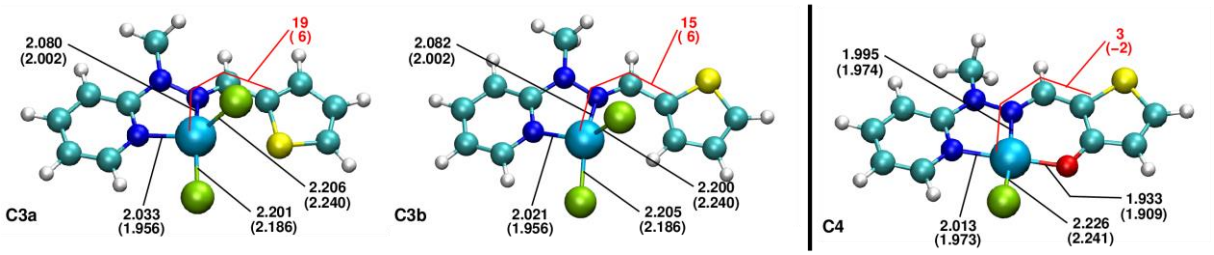

Figure S8. Optimized (RI-TPSS/def2-TZVP) structures of the Cu complexes **C3a**, **C3b**, and **C4**. Selected bond distances and dihedral angles are given (bond distances in Å, angles in °; experimental values in parentheses).

For an analysis of the electronic structure, we recalculated the molecular orbitals of complexes **C3a** and **C4** with CAMY-B3LYP/TZP using the ADF package. For complex **C3a**, the α-spin orbitals are shown in Figure S9, and the β-spin orbitals are depicted in Figure S10. An unambiguous assignment is not possible in all cases, but very roughly speaking, the energetic ordering is such that Cl 3*p* orbitals form the frontier orbitals, followed by π^* unoccupied orbitals on the high-energy side. Below the Cl 3*p* orbitals in energy are π orbitals, followed by orbitals with Cu 3*d* character.

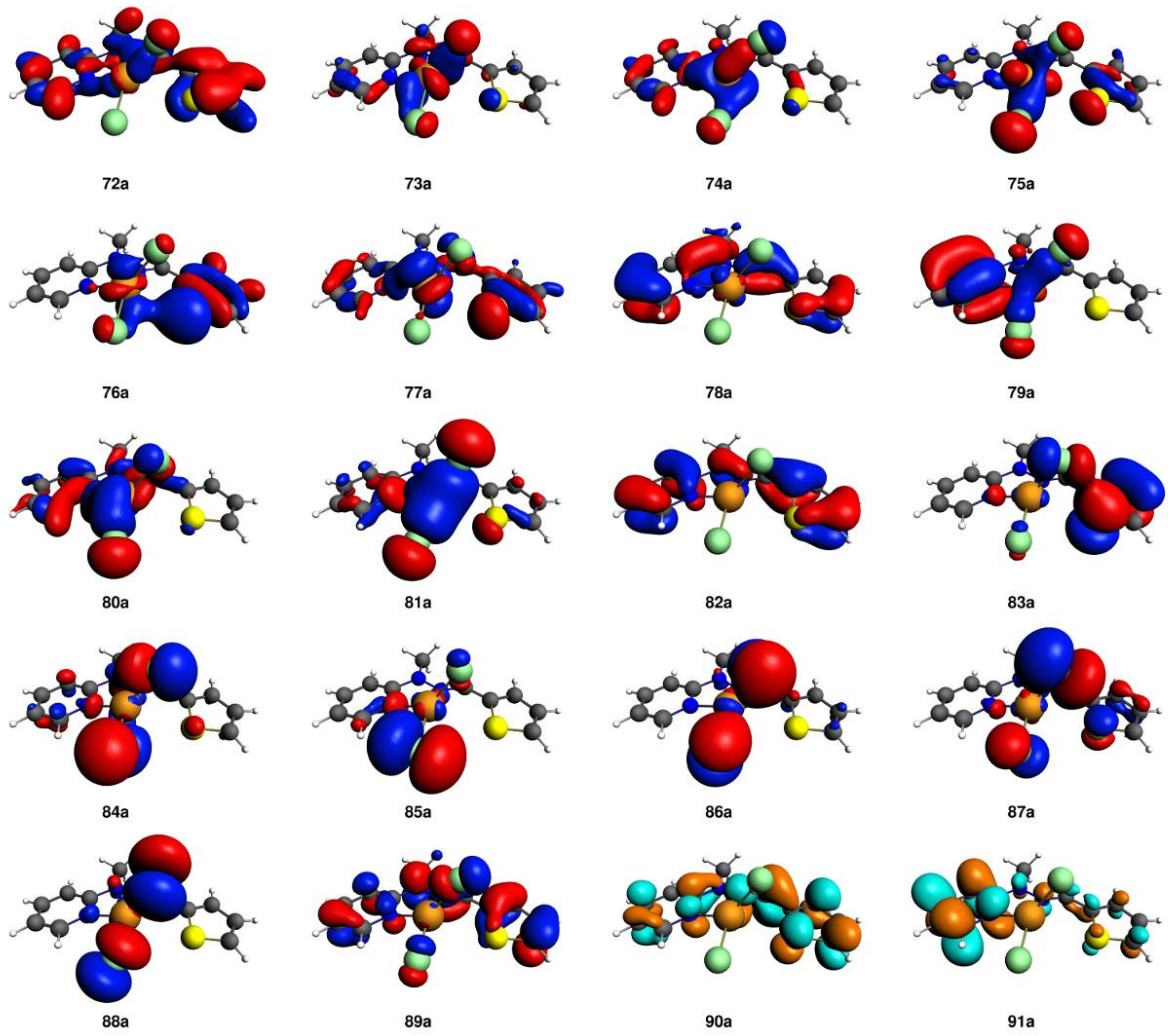

Figure S9. Isosurfaces plots of the α-spin molecular orbitals (CAMY-B3LYP/TZP; isovalue: 0.03) of **C3a**. Occupied orbitals are shown in red/blue, virtual orbitals in orange/turquoise. Orbital 89a corresponds to the SOMO.

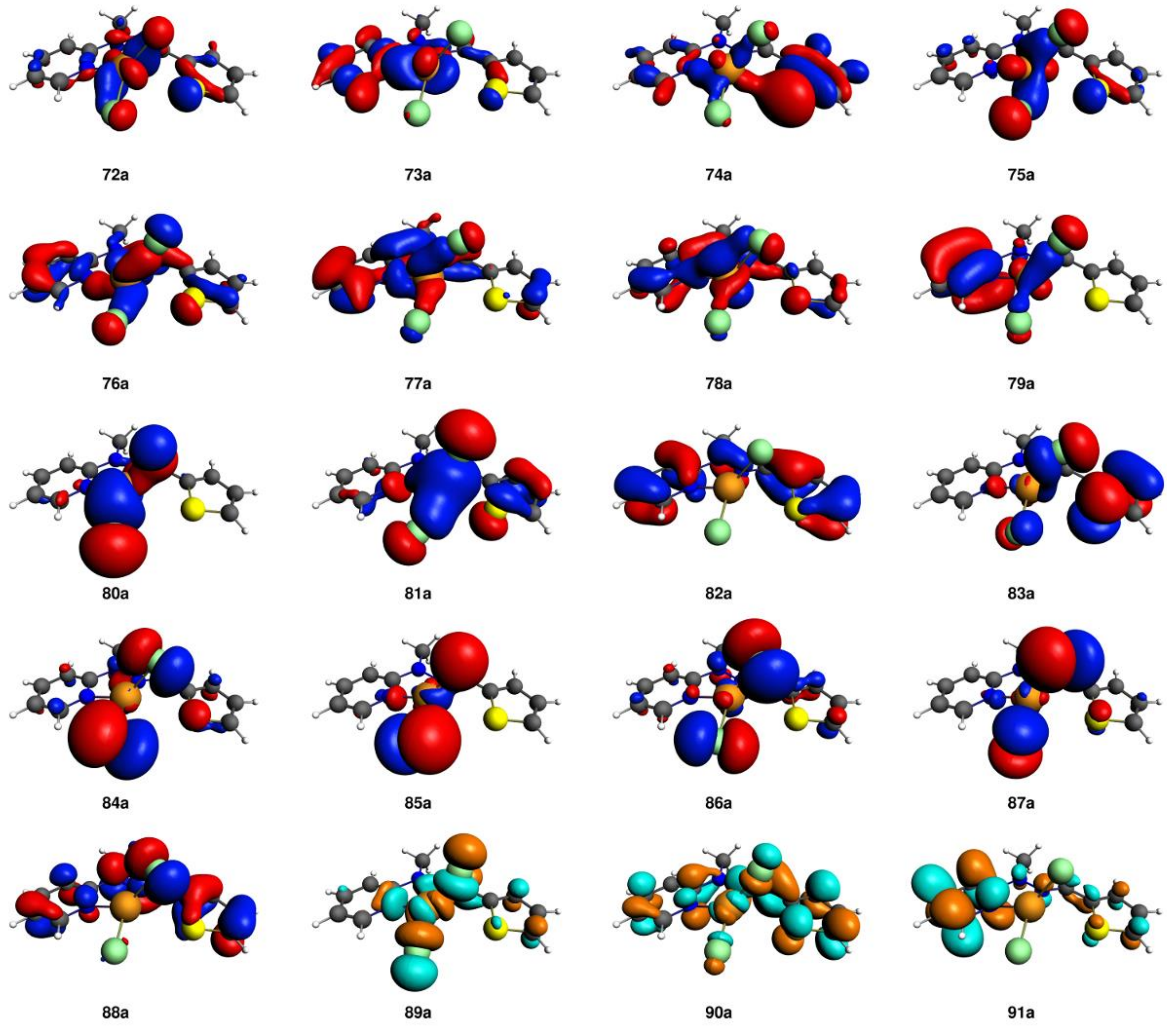

Figure S10. Isosurfaces plots of the β-spin molecular orbitals (CAMY-B3LYP/TZP; isovalue: 0.03) of **C3a**. Occupied orbitals are shown in red/blue, virtual orbitals in orange/turquoise. Orbital 89a corresponds to the SOMO.

Molecule **C4** contains 10 electrons less than **C3**. Hence, orbital 84 corresponds to the SOMO. The α-spin orbitals are illustrated in Figure S11, the β-spin orbitals are shown in Figure S12. The energetic ordering is a bit different here, since π and π^* orbitals appear directly around the HOMO–LUMO gap.

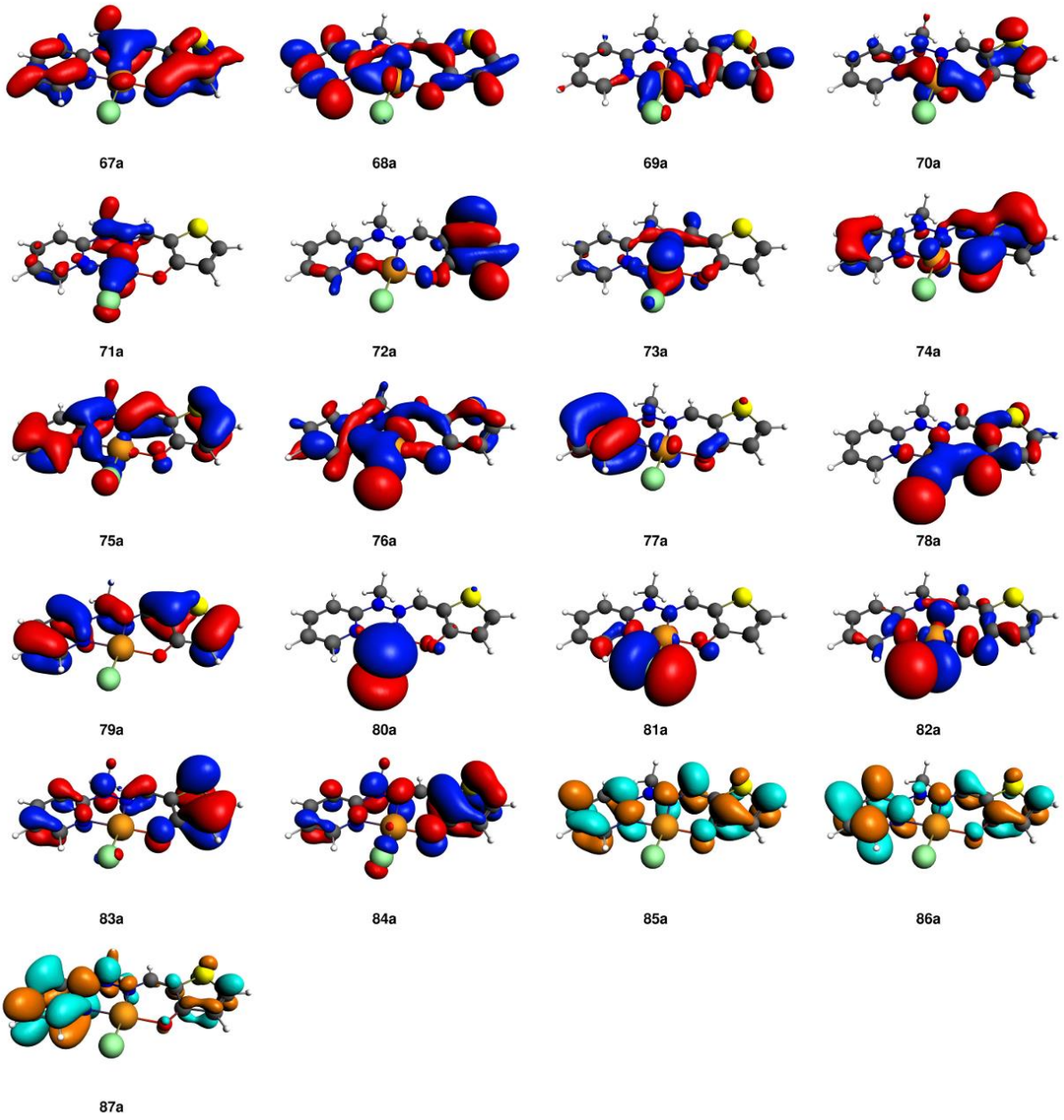

Figure S11. Isosurfaces plots of the α-spin molecular orbitals (CAMY-B3LYP/TZP; isovalue: 0.03) of **C4**. Occupied orbitals are shown in red/blue, virtual orbitals in orange/turquoise. Orbital 84a corresponds to the SOMO.

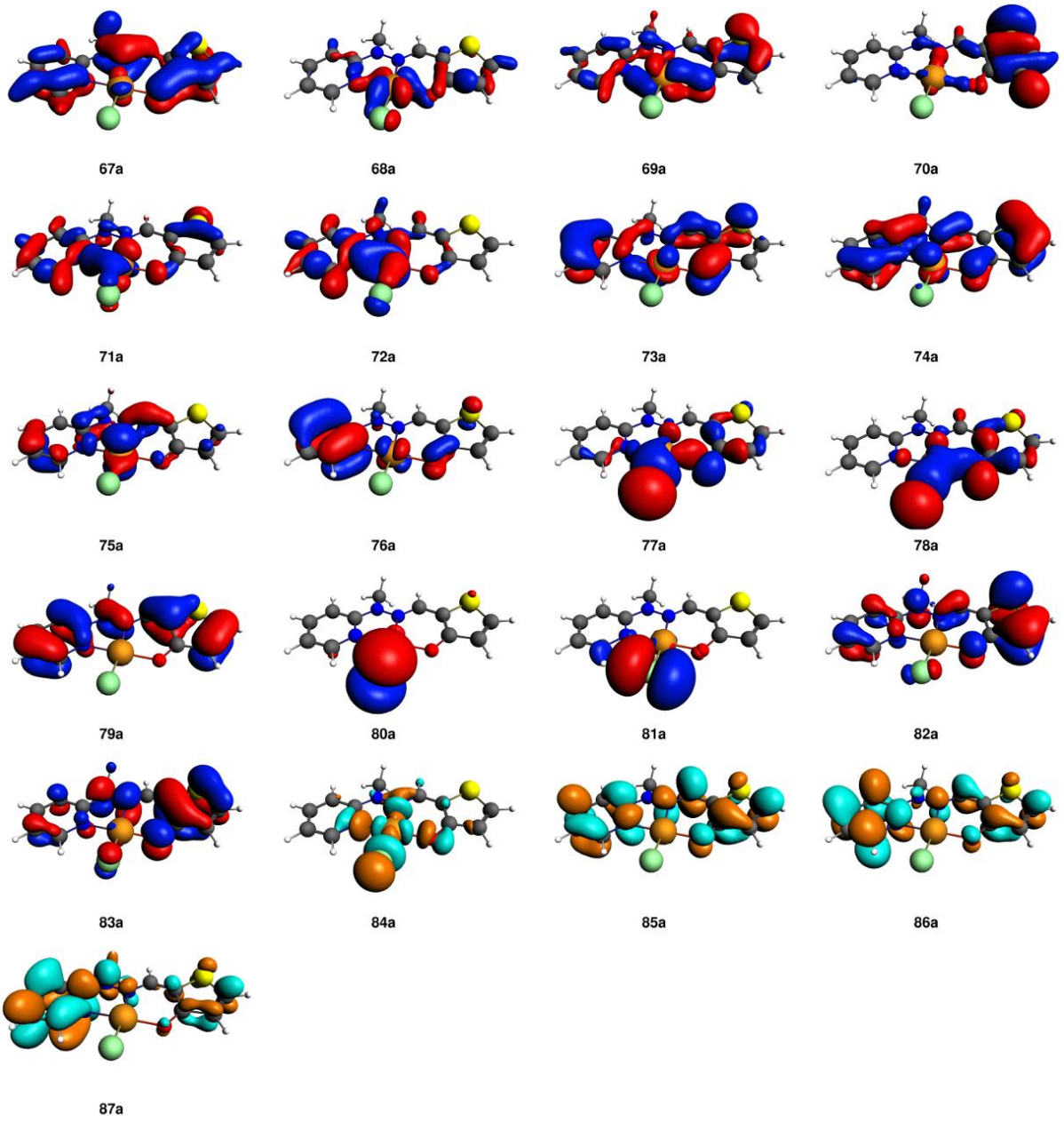

Figure S12. Isosurfaces plots of the β-spin molecular orbitals (CAMY-B3LYP/TZP; isovalue: 0.03) of **C4**. Occupied orbitals are shown in red/blue, virtual orbitals in orange/turquoise. Orbital 84a corresponds to the SOMO.

Excitation energies and UV/Vis-spectra have been calculated on the basis of the unrestricted TDDFT formalism as implemented in ADF (CAMY-B3LYP/TZP) and Q-CHEM (ωB97/6-31G*). The lowest 100 excited states have been considered in all cases. The spectra are shown in Figure S13. Although they differ in detail, the main characteristics are similar. Moreover, the sequence of the peaks and their relative intensities are similar in the calculated spectra and the experimental ones, allowing an approximate assignment of the transitions. However, especially for the shorter-wavelength transitions, this assignment is not unambiguous. An overview over the most prominent excitations of the CAMY-B3LYP/TZP calculation for compounds **C3a** and **C4** is given in Tables S3 and S4.

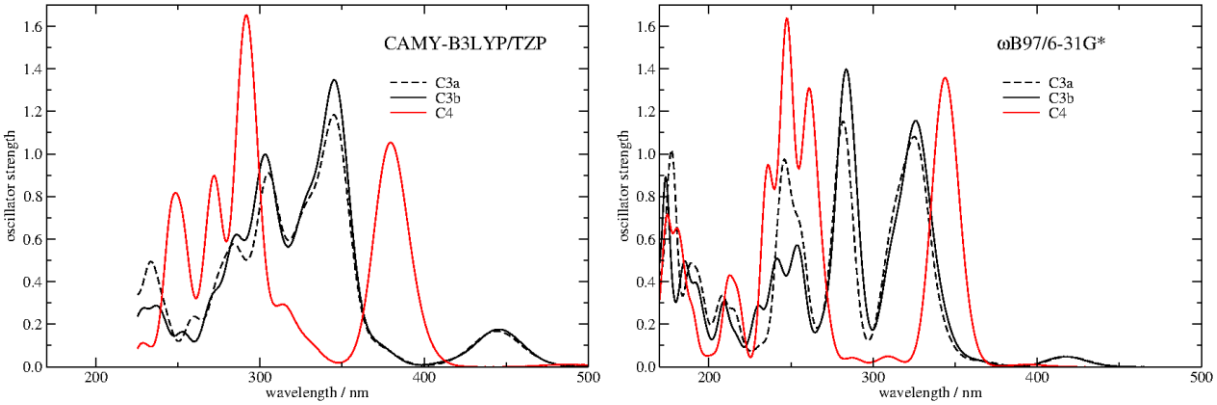

Figure S13. Calculated UV/Vis spectra for molecules **C3a**, **C3b**, and **C4**. Left: CAMY-B3LYP/TZP; right: ωB97/6-31G*.

Table S3. Overview over the most intense among the lowest 100 excitations (CAMY-B3LYP/TZP) for compound **C3a**. Reported are excitation energies (E_{ex}), the corresponding absorption wavelengths λ, oscillator strengths f, dominant orbital transitions (with contribution weights ≥10%), and a rough qualitative assignment for all excitations down to a wavelength of 240 nm with $f \geq 0.03$.

No.	E_{ex} / eV	λ / nm	f	orbital transitions	
8	2.79	444	0.03	$88a_\beta \rightarrow 89a_\beta$ (41%)	$\pi \rightarrow n_{Cl}$ (SOMO)
				$86a_\beta \rightarrow 89a_\beta$ (19%)	$n_{Cl} \rightarrow n_{Cl}$ (SOMO)
14	3.58	346	0.24	$88a_\beta \rightarrow 90a_\beta$ (46%)	$\pi \rightarrow \pi^*$
				$89a_\alpha \rightarrow 90a_\alpha$ (28%)	
17	3.76	330	0.10	$83a_\beta \rightarrow 89a_\beta$ (11%)	$\pi \rightarrow n_{Cl}$ (SOMO)
				$81a_\beta \rightarrow 89a_\beta$ (11%)	$n_{Cl} \rightarrow n_{Cl}$ (SOMO)
19	3.91	317	0.05	$80a_\beta \rightarrow 89a_\beta$ (33%)	$n_{Cl} \rightarrow n_{Cl}$ (SOMO)
21	4.04	307	0.05	$86a_\beta \rightarrow 90a_\beta$ (34%)	$n_{Cl} \rightarrow \pi^*$
22	4.08	304	0.12	$86a_\alpha \rightarrow 90a_\alpha$ (43%)	$n_{Cl} \rightarrow \pi^*$
				$82a_\beta \rightarrow 89a_\beta$ (13%)	$\pi \rightarrow n_{Cl}$ (SOMO)
27	4.36	284	0.09	$88a_\beta \rightarrow 91a_\beta$ (35%)	$\pi \rightarrow \pi^*$
				$89a_\alpha \rightarrow 91a_\alpha$ (35%)	
29	4.53	274	0.06	$84a_\alpha \rightarrow 90a_\alpha$ (36%)	$n_{Cl} \rightarrow \pi^*$
				$84a_\beta \rightarrow 90a_\beta$ (26%)	
				$85a_\alpha \rightarrow 90a_\alpha$ (11%)	
33	4.79	259	0.04	$83a_\beta \rightarrow 90a_\beta$ (47%)	$\pi \rightarrow \pi^*$
				$83a_\alpha \rightarrow 90a_\alpha$ (28%)	

Table S4. Overview over the most intense among the lowest 100 excitations (CAMY-B3LYP/TZP) for compound **C4**. Reported are excitation energies (E_{ex}), the corresponding absorption wavelengths λ, oscillator strengths f, dominant orbital transitions (with contribution weights ≥10%), and a rough qualitative assignment for all excitations down to a wavelength of 240 nm with $f \geq 0.03$.

No.	E_{ex} / eV	λ / nm	f	orbital transitions	
10	3.27	379	0.21	$84a_\alpha \rightarrow 85a_\alpha$ (35%)	$\pi \rightarrow \pi^*$
				$83a_\beta \rightarrow 85a_\beta$ (34%)	
15	3.95	314	0.05	$84a_\alpha \rightarrow 86a_\alpha$ (40%)	$\pi \rightarrow \pi^*$
				$83a_\beta \rightarrow 86a_\beta$ (40%)	
16	4.19	296	0.15	$78a_\beta \rightarrow 84a_\beta$ (47%)	$n_{Cl} \rightarrow n_{Cl}$ (SOMO)
				$77a_\beta \rightarrow 84a_\beta$ (13%)	
				$68a_\beta \rightarrow 84a_\beta$ (13%)	$d_{Cu} \rightarrow n_{Cl}$ (SOMO)
18	4.28	290	0.18	$82a_\beta \rightarrow 85a_\beta$ (35%)	$\pi \rightarrow \pi^*$
				$83a_\alpha \rightarrow 85a_\alpha$ (20%)	
19	4.29	289	0.07	$83a_\alpha \rightarrow 85a_\alpha$ (22%)	$\pi \rightarrow \pi^*$
22	4.54	273	0.11	$77a_\beta \rightarrow 84a_\beta$ (32%)	$n_{Cl} \rightarrow n_{Cl}$ (SOMO)
				$78a_\beta \rightarrow 85a_\beta$ (13%)	$n_{Cl} \rightarrow \pi^*$
24	4.57	271	0.05	$77a_\beta \rightarrow 84a_\beta$ (17%)	$n_{Cl} \rightarrow n_{Cl}$ (SOMO)
				$82a_\alpha \rightarrow 86a_\alpha$ (13%)	$n_{Cl} \rightarrow \pi^*$
				$80a_\beta \rightarrow 85a_\beta$ (10%)	
32	4.90	253	0.11	$83a_\beta \rightarrow 87a_\beta$ (34%)	$\pi \rightarrow \pi^*$
				$84a_\alpha \rightarrow 87a_\alpha$ (31%)	
34	5.04	246	0.12	$82a_\beta \rightarrow 86a_\beta$ (22%)	$\pi \rightarrow \pi^*$
				$83a_\alpha \rightarrow 86a_\alpha$ (18%)	
				$79a_\alpha \rightarrow 85a_\alpha$ (14%)	

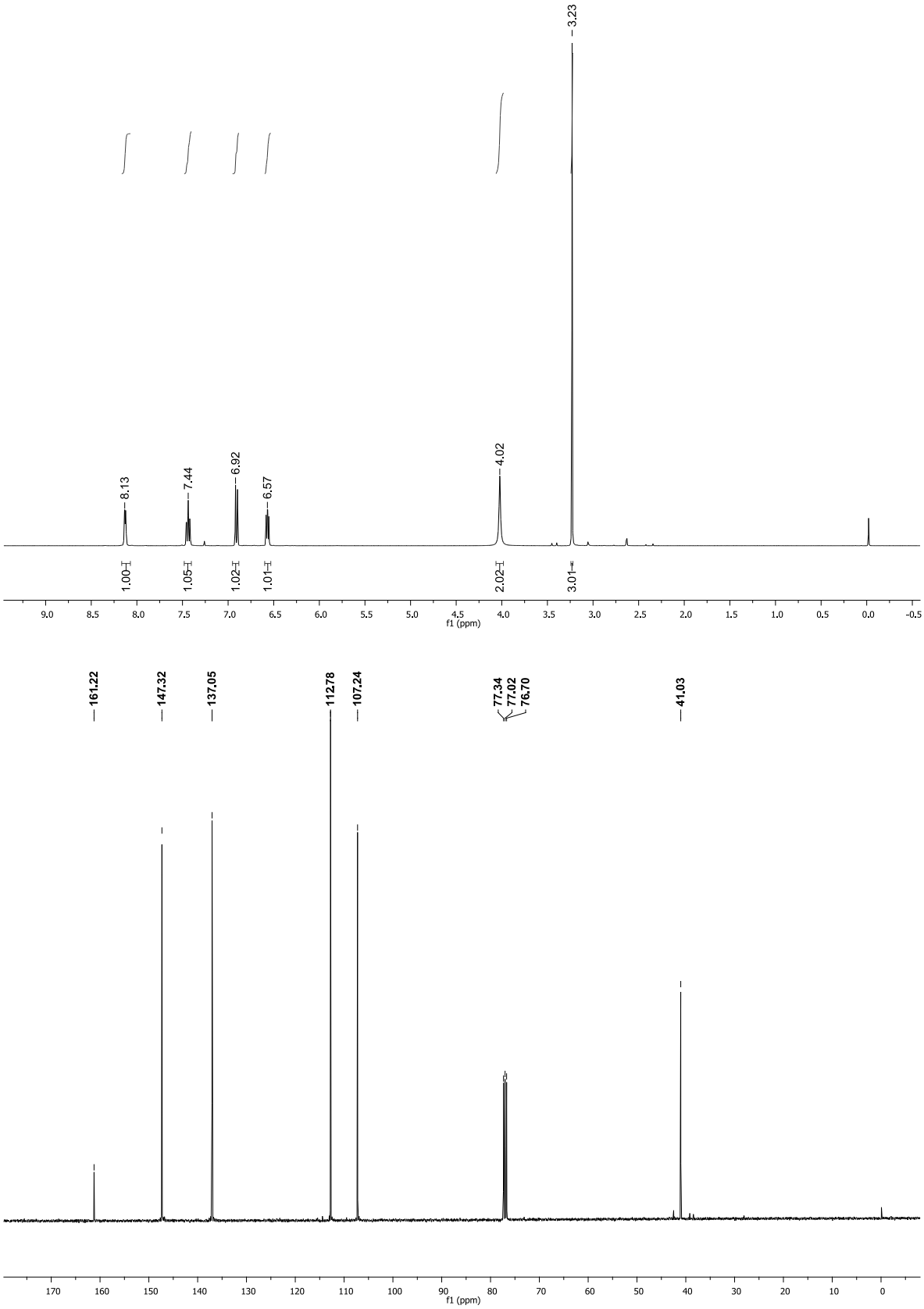

Figure S14. ^{1}H and ^{13}C NMR spectra ($CDCl_3$) of compound **1**.

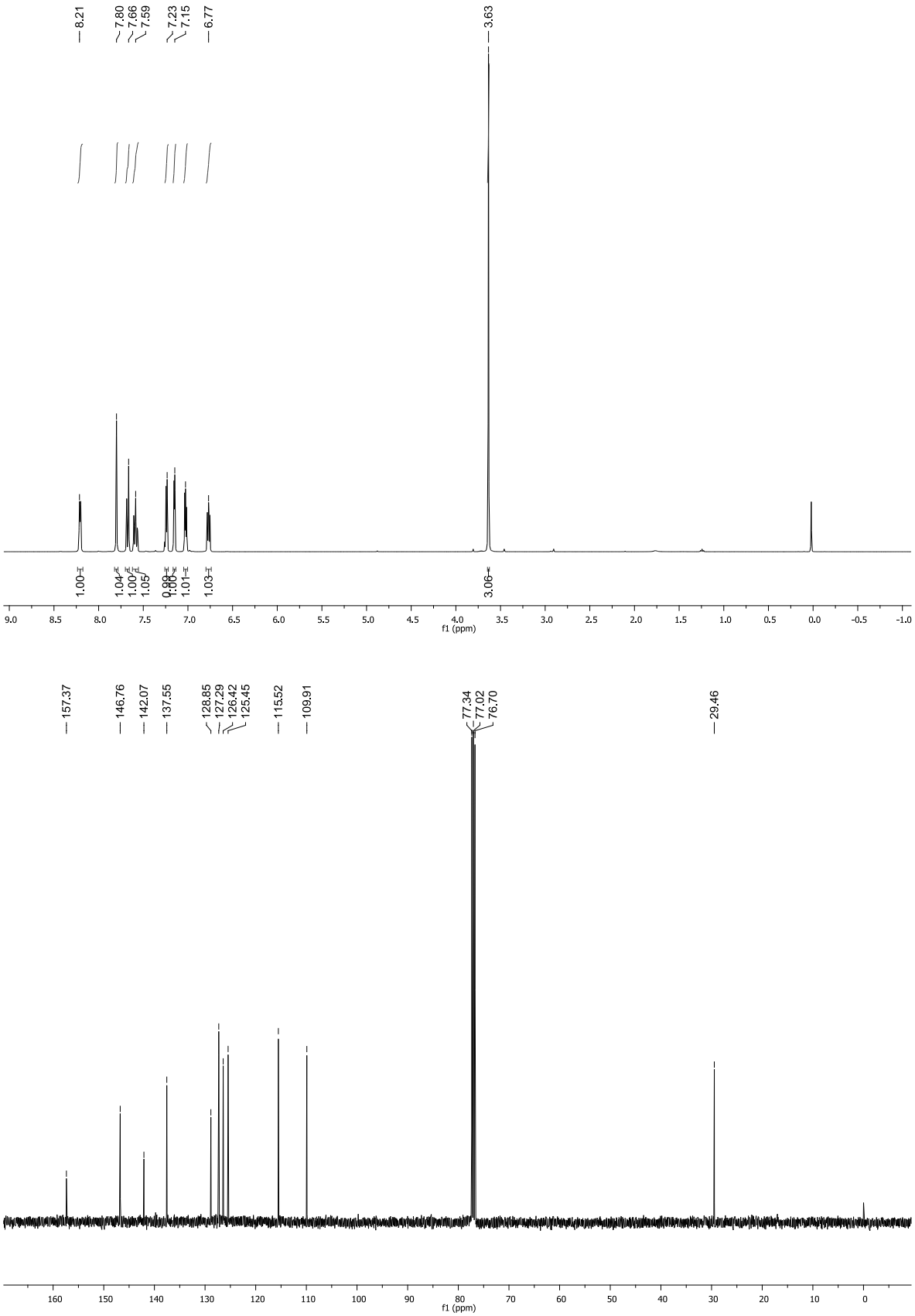

Figure S15. ^{1}H and ^{13}C NMR spectra ($CDCl_3$) of compound **2**.

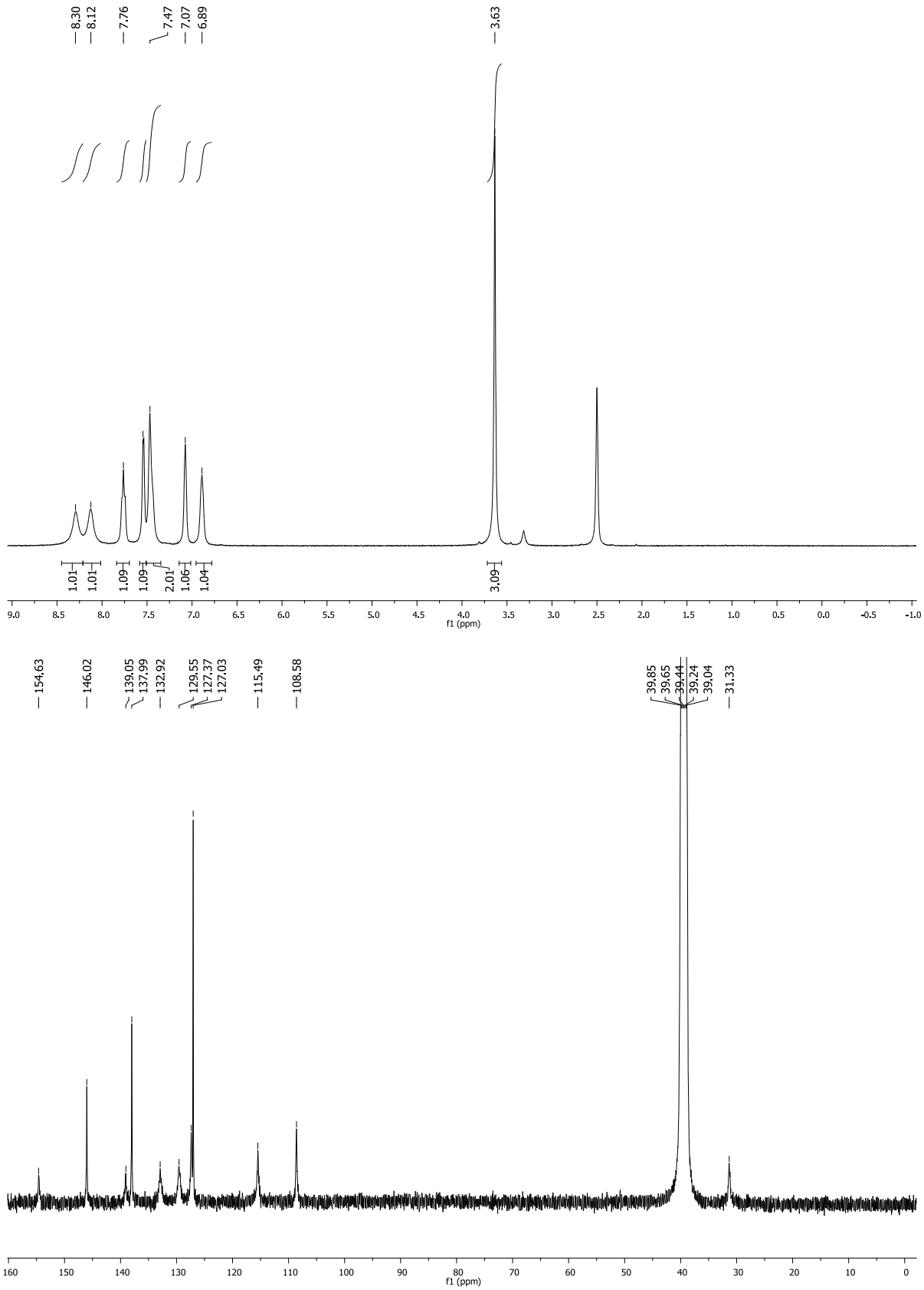

Figure S16. ^{1}H and ^{13}C NMR spectra (DMSO-d_6) of compound **5**.

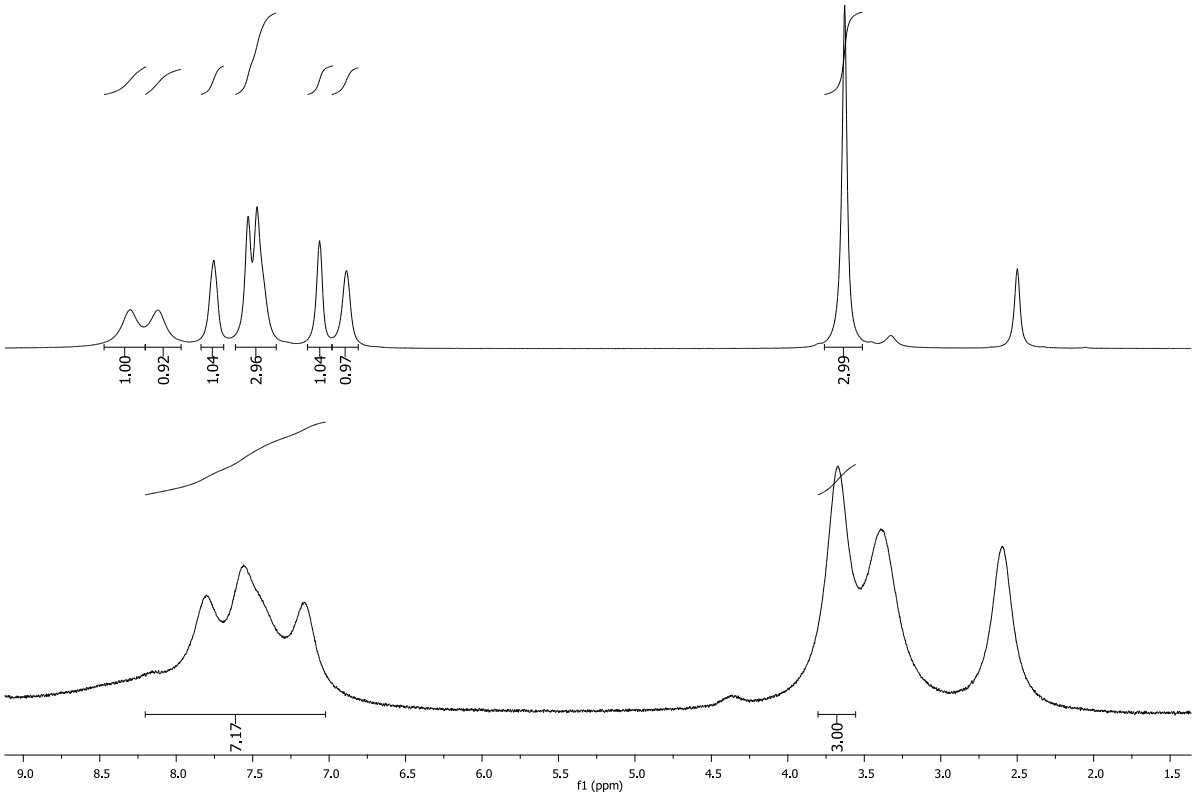

Figure S17. ^{1}H NMR spectra (DMSO-d_6) of Cu(I)-containing [Cu(**2**)I]$_2$ (compound **5**, top) and [Cu(**2**)Cl] (compound **6**, bottom). The paramagnetism of the oxidized copper(II) decomposition product of compound **6** leads to broader signals in the ^{1}H NMR spectrum (bottom).